Beyond Euclidean: Dual-Space Representation Learning for Weakly Supervised Video Violence Detection

Jiaxu Leng^{1,2}, **Zhanjie Wu**^{1,2}, **Mingpi Tan**^{1,2}, **Yiran Liu**^{1}, **Ji Gan**^{1,2},
Haosheng Chen^{1,2}, **Xinbo Gao** ^{1,2} *

^{1} Chongqing University of Posts and Telecommunications, Chongqing, China
^{2} Chongqing Institute for Brain and Intelligence, Guangyang Bay Laboratory, Chongqing, China
gaoxb@cqupt.edu.cn

Abstract

While numerous Video Violence Detection (VVD) methods have focused on representation learning in Euclidean space, they struggle to learn sufficiently discriminative features, leading to weaknesses in recognizing normal events that are visually similar to violent events (*i.e.*, ambiguous violence). In contrast, hyperbolic representation learning, renowned for its ability to model hierarchical and complex relationships between events, has the potential to amplify the discrimination between visually similar events. Inspired by these, we develop a novel Dual-Space Representation Learning (DSRL) method for weakly supervised VVD to utilize the strength of both Euclidean and hyperbolic geometries, capturing the visual features of events while also exploring the intrinsic relations between events, thereby enhancing the discriminative capacity of the features. DSRL employs a novel information aggregation strategy to progressively learn event context in hyperbolic spaces, which selects aggregation nodes through layer-sensitive hyperbolic association degrees constrained by hyperbolic Dirichlet energy. Furthermore, DSRL attempts to break the cyber-balkanization of different spaces, utilizing cross-space attention to facilitate information interactions between Euclidean and hyperbolic space to capture better discriminative features for final violence detection. Comprehensive experiments demonstrate the effectiveness of our proposed DSRL.

1 Introduction

Compared with manually checking out violent events in surveillance videos which is time-consuming and laborious, Video Violence Detection (VVD), which focuses on identifying violent events in videos and provides automatic and instantaneous responses, has gained significant research attention due to its potential applications. However, it is expensive to annotate each frame in a video so that we can train a VVD model with supervised learning. To address this, current methods often utilize weakly supervised settings to formulate the problem as a multiple-instance learning (MIL)[19] task. These methods treat a video as a bag of instances (*i.e.,* snippets or segments), and predict their labels based on the video-level annotations.

According to the modality type of the input data, existing weakly supervised VVD methods can be roughly divided into two categories, unimodal with only vision input and multimodal with vision and audio input. The unimodal methods [29, 36, 8, 10, 20] learn the different distributions of normal and violent events through video-level labels, focus on finding valuable visual cues that are distinct from non-violent events and use them to detect violent events, *i.e.,* fighting. However, relying on visual cues

*Corresponding author

38th Conference on Neural Information Processing Systems (NeurIPS 2024).

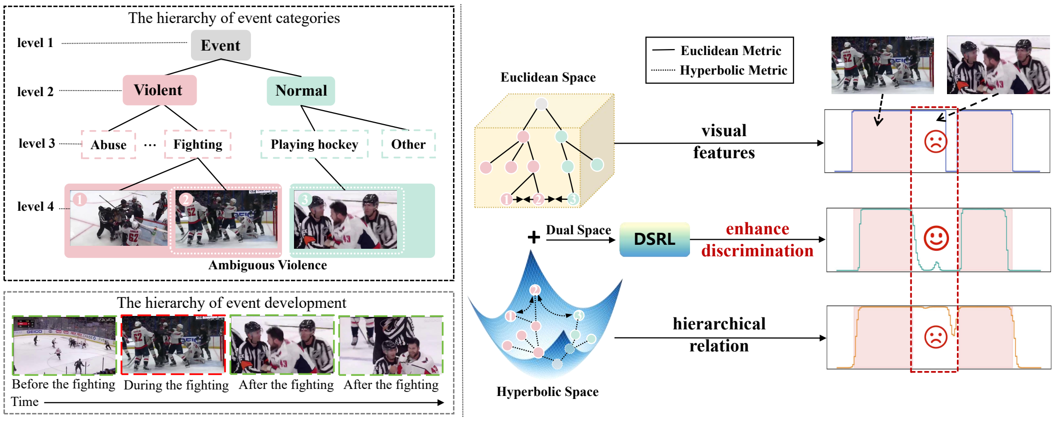

(a) Hierarchical Diagram in VVD

(b) Superiority of DSRL for Ambiguous Violence Detection

Figure 1: (a) Hierarchical diagram in Video Violence Detection (VVD). (b) Our DSRL enhances the detection of ambiguous violence by combining Euclidean and Hyperbolic spaces to balance visual feature expression and hierarchical event relations.

to identify violent events is sometimes unreliable, especially when facing visually ambiguous events, like normal physical collisions and fighting behavior in hockey games. To alleviate this problem, Wu et al [34] released a large multimodal violence dataset, named XD-Violence, and accelerated a series of multimodal VVD methods [34, 35, 22, 37, 23]. Multimodal VVD methods incorporate not only visual cues but also complementary audio information for improving the discrimination of violent events. Previous methods have employed Euclidean space representation learning and achieved good results in many other computer vision tasks[27, 28, 15, 32]. Despite advancements in audio-visual violent video detection (VVD) methods, their performance remains unsatisfactory in recognizing normal events that are visually similar to violent events (i.e., ambiguous violence) due to the limitations of Euclidean space. While visual features are fully extracted in Euclidean space, these methods fail to adequately capture and utilize the intrinsic relations between events.

To fully understand an event, on the one hand, we need to explore the hierarchy of event categories, on the other hand, we need to sort through the events, including the trend before the event, the action during the event and the behaviour after the event, which reflects the hierarchy of event development, shown in Figure 1(a). An ambiguous violent event is confusing at the current category level or happening moment, but may easily be detected if we can grasp the hierarchical relations. Fortunately, hyperbolic representation learning, characterized by exponentially increasing the metric distances and naturally reflects the hierarchical structure of data, has gained attention and shown promising performance in computer vision tasks, like semantic segmentation [1], medical image recognition [38], action recognition [24, 17], anomaly recognition [12]. At present, only one method, HyperVD [25], makes a preliminary attempt on the VVD task via hyperbolic representation learning. HyperVD introduces the Hyperbolic Graph Convolutional Networks (HGCN) [3], an extended version of Euclidean graph convolution for representation learning in hyperbolic space, to learn discriminative representations. However, HGCN employs a hard node selection strategy during the message passing, where the nodes whose correlation is higher than the threshold (a manual parameter) are selected for message aggregation and otherwise discarded, which leads to insufficient hierarchical relation learning. In addition, existing VVD methods deploy feature embedding either in Euclidean or hyperbolic spaces. Representation learning in a single space is like picking the sesame and losing the watermelon, where the feature embedding is insufficient to guarantee the performance of VVD. On the one hand, hyperbolic representation learning strengthens the hierarchical relation of events but weakens the expression of visual features, on the other hand, Euclidean representations emphasize visual features but ignore relations between events. Therefore, leveraging the advantages of both spaces is essential for improving the performance of VVD methods, shown in Figure 1(b).

In this paper, we propose a novel Dual-Space Representation Learning (DSRL) method for weakly supervised VVD under the multimodal input setting. Specifically, we designed two customized modules, the Hyperbolic Energy-constrained Graph Convolutional Network module (HE-GCN) and the Dual-Space Interaction module (DSI). Instead of adopting the hard node selection strategy in HGCN, HE-GCN selects nodes for message aggregation by our introduced layer-sensitive hyperbolic association degrees, which are dynamic thresholds determined by the message aggregation degree at each layer. To better align with the characteristics of hyperbolic spaces, we introduce the hyperbolic Dirichlet energy to quantify the extent of message aggregation. Benefiting from the dynamic threshold, the layer-by-layer focused message passing strategy adopted by HE-GCN not only ensures the efficiency of information excavation but also improves the model's comprehensive understanding of the events, thus enhancing the model's ability to discriminate ambiguous violent events. Although hyperbolic representation learning enhances the understanding of hierarchical relations of events, the role of visual representations in violence detection cannot be discarded. However, fusing representation in different spaces remains a challenge, to break the information cocoon, DSI utilises cross-space attention to facilitate information interactions between Euclidean and hyperbolic space to capture better discriminative features, where Euclidean representations have effectiveness on the significant motion and shape changes in the video, while hyperbolic representations accelerate the comprehension of hierarchical relations between events, working together to improve the performance of violence detection in videos.

Contributions: **(1)** To the best of our knowledge, our DSRL is the first method to integrate Euclidean and hyperbolic geometries for VVD, significantly improving discrimination of ambiguous violence and achieving state-of-the-art performance on the XD-Violence dataset in both unimodal and multimodal settings. **(2)** To better capture the hierarchical context of events, we design the HE-GCN module with a novel message aggregation strategy, where the node selection threshold is dynamic not fixed and determined by layer-sensitive hyperbolic association degrees based on hyperbolic Dirichlet energy. **(3)** To break the information cocoon for better dual-space cooperation, visual discrimination from Euclidean and event hierarchical discrimination from hyperbolic, we propose the DSI module, which utilizes cross-space attention to facilitate information interactions.

2 Related Work

Weakly Supervised Video Violence Detection. Weakly supervised VVD requires identifying violent snippets under video-level labels, where the MIL [19] framework is widely used for denoising irrelevant information. Recently, progress has been made in weakly supervised VVD, with approaches categorized into two main categories: vision-based and audio-visual-based methods. Employing exclusively visual cues, vision-based VVD endeavours to discern the occurrence of violent events within videos. Most existing works [7, 26, 30, 33] consider VVD as solely a visual task, and CNN-based networks are utilized to encode visual features. However, these approaches overlook the interaction between different modalities and the relevant audio information, which could negatively impact the accuracy of violence detection. To alleviate this problem, Wu et al [34] released a large multimodal violence dataset, named XD-Violence, and accelerated a series of multimodal VVD methods [34, 35, 22, 37, 23, 18, 25]. In contrast to unimodal methods, they incorporate not only visual cues but also complementary audio information for improving the discrimination of ambiguous violent events. Subsequently, many studies [22, 23] have focused on the integration of visual and audio information. There is also work[37] focused on solving the modality asynchrony problem. Despite the progress of weakly supervised multimodal VVD methods, all the above methods carry out representation learning in Euclidean Spaces, making it difficult to effectively handle ambiguous violence.

Hyperbolic Representation Learning. Hyperbolic representation learning, characterized by exponentially increasing the metric distances and naturally reflects the hierarchical structure of data, has gained attention and shown promising performance in computer vision tasks, like semantic segmentation [1], visual representation learning [9], medical image recognition [38], action recognition [24, 17], anomaly recognition [12]. More Recently, HyperVD [25] has made an initial attempt at the VVD task using hyperbolic representation learning. HyperVD incorporates Hyperbolic Graph Convolutional Networks (HGCN) [3] to acquire discriminative representations. However, while hyperbolic representation learning enhances the hierarchical relationships of events, it diminishes the representation of visual features. Therefore, we propose a novel Dual-Space Representation Learning to joint the strengths of Euclidean and hyperbolic space. Meanwhile, we design HE-GCN to gradually shift its focus from capturing global contextual information to concentrating on crucial detailed features, progressively capturing the hierarchical context of events.

3 Preliminaries

Problem Definition. Given an video sequence $S = \{S_t\}_{t=1}^{T}$ with T non-overlapping segments. For a video segment, the weakly supervised VVD requires distinguishing whether it contains violent events via an events relevance label $y_t \in \{0, 1\}$, where $y_t = 1$ means in the current segment includes violent cues.

Hyperbolic Geometry. A Riemannian manifold $(\mathcal{M}, g)$ of dimension *n* is a real and smooth manifold equipped with an inner product on tangent space g_x: $\mathcal{T}_x\mathcal{M} \times \mathcal{T}_x\mathcal{M} \to \mathbb{R}$ at each point $x \in \mathcal{M}$, where the tangent space $\mathcal{T}_x\mathcal{M}$ is a n-dimensional vector space and can be seen as a first-order local approximation of $\mathcal{M}$ around point x. In particular, hyperbolic space $(\mathbb{D}_c^n, g^c)$, a constant negative curvature Riemannian manifold, is defined by the manifold $\mathbb{D}_c^n = \{x \in \mathbb{R}^n : c\,\|x\| < 1\}$ equipped with the following Riemannian metric:$g_x^c = \lambda_x^2 g^E$, where $\lambda_x := \frac{2}{1-c\|x\|^2}$ and $g^E = I_n$ is the Euclidean metric tensor. Considering the numerical stability and calculation simplicity of its exponential and logarithmic maps and distance functions, we select the Lorentz model [21] as the framework cornerstone.

Lorentz Model. Formally, an n-dimensional Lorentz model is the Riemannian manifold $\mathbb{L}_K^n = \left(\mathcal{L}^n, \mathfrak{g}_{\mathbf{x}}^K\right)$. K is the constant negative curvature. $\mathfrak{g}_{\mathbf{x}}^K = diag\left(-1, 1, \cdots, 1\right)$ is the Riemannian metric tensor. We denote $\mathcal{L}^n$ as the n-dimensional hyperboloid manifold with constant negative curvature K:

$$\mathcal{L}^n := \left\{\mathbf{x} \in \mathbb{R}^{n+1} : \langle \mathbf{x}, \mathbf{x} \rangle_{\mathcal{L}} = \frac{1}{K}, x_0 > 0\right\}. \tag{1}$$

Let $\mathbf{x}, \mathbf{y} \in \mathbb{R}^{n+1}$, then the Lorentzian scalar product is defined as:

$$\langle \mathbf{x}, \mathbf{y} \rangle_{\mathcal{L}} := -x_0 y_0 + \sum_{i=1}^{n} x_i y_i, \tag{2}$$

where $\mathcal{L}^n$ is the upper sheet of hyperboloid in an (n+1)-dimensional Minkowski space with the origin $\left(\sqrt{-1/K}, 0, \cdots, 0\right)$. For simplicity, we denote point x in the Lorentz model as $x \in \mathbb{L}_K^n$.

Tangent Space. Given the tangent space at x is defined as an n-dimensional vector space approximating $\mathbb{L}_K^n$ around x,

$$\mathcal{T}_{\mathbf{x}}\mathbb{L}_K^n := \left\{\mathbf{y} \in \mathbb{R}^{n+1} \mid \langle \mathbf{y}, \mathbf{x} \rangle_{\mathcal{L}} = 0\right\}. \tag{3}$$

Note that $\mathcal{T}_{\mathbf{x}}\mathbb{L}_K^n$ is a Euclidean subspace of $\mathbb{R}^{n+1}$. Particularly, we denote the tangent space at the origin as $\mathcal{T}_{\mathbf{0}}\mathbb{L}_K^n$.

Logarithmic and Exponential Maps. The mapping between hyperbolic spaces and tangent spaces can be done by exponential map and logarithmic map. The exponential map is a map from a subset of a tangent space of $\mathbb{L}_K^n$(i.e., $\mathcal{T}_{\mathbf{x}}\mathbb{L}_K^n$) to $\mathbb{L}_K^n$ itself. The logarithmic map is the reverse map that maps back to the tangent space. For points $\mathbf{x}, \mathbf{y} \in \mathbb{L}_K^n$, $\mathbf{v} \in \mathcal{T}_{\mathbf{x}}\mathbb{L}_K^n$, such that $\mathbf{v} \neq \mathbf{0}$ and $\mathbf{x} \neq \mathbf{y}$, the exponential map $\exp_{\mathbf{x}}^K(\cdot)$ and logarithmic map $\log_{\mathbf{x}}^K(\cdot)$ are given as follows:

$$\exp_{\mathbf{x}}^K(\mathbf{v}) = \cosh(\sqrt{-K}\,\|\mathbf{v}\|_{\mathcal{L}})\mathbf{x} + \sinh(\sqrt{-K}\,\|\mathbf{v}\|_{\mathcal{L}})\frac{\mathbf{v}}{\sqrt{-K}\,\|\mathbf{v}\|_{\mathcal{L}}} \tag{4}$$

$$\log_{\mathbf{x}}^K(\mathbf{y}) = d_{\mathbb{L}}^K(\mathbf{x}, \mathbf{y})\,\frac{\mathbf{y} - K\langle \mathbf{x}, \mathbf{y} \rangle_{\mathcal{L}}}{\left\|\mathbf{y} - K\langle \mathbf{x}, \mathbf{y} \rangle_{\mathcal{L}}\right\|_{\mathcal{L}}}, \tag{5}$$

where$\|\mathbf{v}\|_{\mathcal{L}} = \sqrt{\langle \mathbf{v}, \mathbf{v} \rangle_{\mathcal{L}}}$ denotes Lorentzian norm of $\mathbf{v}$ and $d_{\mathcal{L}}^K(\cdot, \cdot)$ denotes the Lorentzian intrinsic distance function between two points $\mathbf{x}, \mathbf{y} \in \mathbb{L}_K^n$, which is given as:

$$d_{\mathcal{L}}^K(\mathbf{x}, \mathbf{y}) = arcosh\left(K\langle \mathbf{x}, \mathbf{y} \rangle_{\mathcal{L}}\right). \tag{6}$$

4 Methodology

In this paper, we propose the Dual-Space Representation Learning (DSRL) method to improve the discrimination of ambiguous violence. Within DSRL, we first design the Hyperbolic Energy-constrained Graph Convolutional Network Module (HE-GCN) to better capture the hierarchical context of events (Sec. 4.1). Then, the Dual-Space Interaction Module (DSI) is introduced to break the information cocoon for better dual-space cooperation (Sec. 4.2). An illustration of the main components of DSRL is provided in Figure 2.

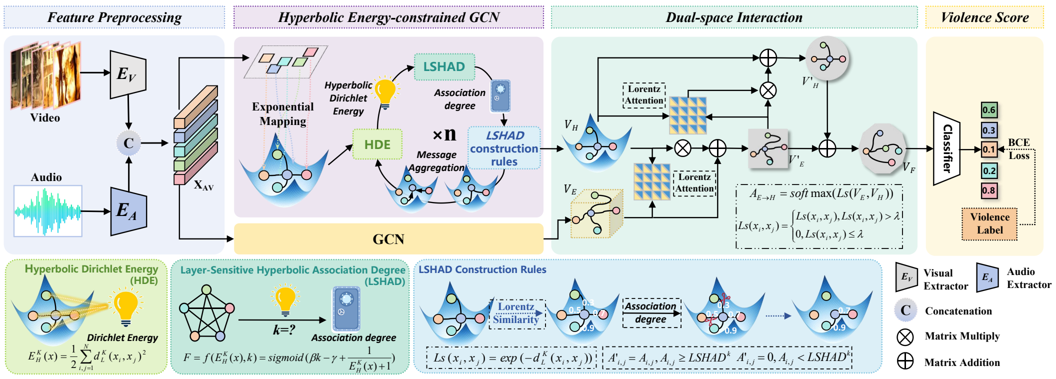
Feature Preprocessing
Hyperbolic Energy-constrained GCN
Dual-space Interaction
Violence Score
Video
E_V
C
Audio
E_A
X_{AV}
Exponential Mapping
Hyperbolic Dirichlet Energy
LSHAD
Association degree
×n
HDE
Message Aggregation
LSHAD construction rules
GCN
V_H
V_E
Lorentz Attention
Lorentz Attention
V'_H
V'_E
V_F
$A_{E\to H} = soft\max(Ls(V_E, V_H))$
$Ls(x_i,x_j)=\begin{cases}Ls(x_i,x_j), Ls(x_i,x_j)>\lambda\\0, Ls(x_i,x_j)\le\lambda\end{cases}$
Classifier
0.6
0.3
0.1
0.2
0.8
BCE Loss
Violence Label
Hyperbolic Dirichlet Energy (HDE)
Dirichlet Energy
$E_H^K(x)=\frac{1}{2}\sum_{i,j=1}^{N} d_L^K(x_i,x_j)^2$
Layer-Sensitive Hyperbolic Association Degree (LSHAD)
k=?
Association degree
$F = f(E_H^K(x),k) = sigmoid(\beta k - \gamma + \frac{1}{E_H^K(x)+1})$
LSHAD Construction Rules
Lorentz Similarity
0.5
0.3
0.7
0.9
Association degree
$Ls(x_i,x_j) = exp(-d_L^K(x_i,x_j))$
$A'_{i,j} = A_{i,j}, A_{i,j} \ge LSHAD^k \quad A'_{i,j} = 0, A_{i,j} < LSHAD^k$
E_V Visual Extractor
E_A Audio Extractor
C Concatenation
⊗ Matrix Multiply
⊕ Matrix Addition

Figure 2: A conceptual diagram of our DSRL.

4.1 Hyperbolic Energy-constrained Graph Convolutional Network Module (HE-GCN)

HE-GCN primarily involves mapping features from Euclidean space to hyperbolic space, then transforming the features, constructing the message graph by calculating hyperbolic Dirichlet energy and Layer-Sensitive Hyperbolic Association Degree, and finally aggregating messages to obtain the new feature graph.

Mapping from Euclidean to hyperbolic spaces. Let $\left\{x_i^E\right\}_{i\in\mathcal{V}}$ be input Euclidean node features, and $\mathbf{o} := [1, 0, \cdots, 0]$ denote the origin on the manifold $\mathcal{L}$ of the Lorenzt model. There is $\left\langle \mathbf{o}, \left[0, x_i^E\right]\right\rangle_{\mathcal{L}} = 0$, where $\langle\cdot,\cdot\rangle_{\mathcal{L}}$ denotes the Lorentz inner product defined in Eq. 2. We can reasonably regard $\left[0, x_i^E\right]$ as a node on the tangent space at the origin $\mathbf{o}$. HE-GCN uses the exponential map defined in Eq. 4 to generate hyperbolic node representations on the Lorentz model:

$$x_i^{\mathcal{L}} = \exp_{\mathbf{o}}\left(\left[0, x_i^E\right]\right) = \left[cosh\left(\left\|x_i^E\right\|_2\right), sinh\left(\left\|x_i^E\right\|_2\right)\frac{x_i^E}{\left\|x_i^E\right\|_2}\right]. \tag{7}$$

Hyperbolic Feature Transformation. According to [5], we reformalize the lorentz linear layer to learn a matrix $\mathbf{M} = \begin{bmatrix}\mathbf{v}^\top\\ \mathbf{W}\end{bmatrix}$, $\mathbf{v} \in \mathbb{R}^{n+1}$, $\mathbf{W} \in \mathbb{R}^{m\times(n+1)}$ satisfying $\forall\mathbf{x} \in \mathbb{L}^n$, $f_{\mathbf{x}}(\mathbf{M})\mathbf{x} \in \mathbb{L}^m$, where $f_{\mathbf{x}} : \mathbb{R}^{(m+1)\times(n+1)} \to \mathbb{R}^{(m+1)\times(n+1)}$ should be a function that maps any matrix to a suitable one for the hyperbolic linear layer. Specifically, $\forall\mathbf{x} \in \mathbb{L}_K^n$, $\mathbf{M} \in \mathbb{R}^{(m+1)\times(n+1)}$, $f_{\mathbf{x}}(\mathbf{M})$ is given as

$$f_{\mathbf{x}}(\mathbf{M}) = f_{\mathbf{x}}\left(\begin{bmatrix}\mathbf{v}^\top\\ \mathbf{W}\end{bmatrix}\right) = \begin{bmatrix}\frac{\sqrt{\|W\mathbf{x}\|^2-1/K}}{\mathbf{v}^\top\mathbf{x}}\mathbf{v}^\top\\ \mathbf{W}.\end{bmatrix} \tag{8}$$

Theorem 1 *$\forall\boldsymbol{x} \in \mathbb{L}^n$, $\boldsymbol{M} \in \mathbb{R}^{(m+1)\times(n+1)}$, we have $f_x(\boldsymbol{M})\boldsymbol{x} \in \mathbb{L}_K^m$.*

For simplicity, we use a morel general formula $*$ of hyperbolic linear layer for feature transformation based on $f_{\mathbf{x}}\left(\begin{bmatrix}\mathbf{v}^\top\\ \mathbf{W}\end{bmatrix}\right)\mathbf{x}$ with activation, dropout, bias and normalization,

$$\mathbf{y} = HL\left(\mathbf{x}\right) = \begin{bmatrix}\sqrt{\left\|\phi\left(\mathbf{Wx}, \mathbf{v}\right)\right\|^2 - 1/K}\\ \phi\left(\mathbf{Wx}, \mathbf{v}\right),\end{bmatrix} \tag{9}$$

where $\mathbf{x} \in \mathbb{L}_K^n$, $\mathbf{W} \in \mathbb{R}^{m\times(n+1)}$, $\mathbf{v} \in \mathbb{R}^{n+1}$ denotes a velocity (ratio to the speed of light) in the Lorentz transformations, and ϕ is an operation function: for the dropout, the function is $\phi\left(\mathbf{Wx}, \mathbf{v}\right) = \mathbf{W}dropout\left(\mathbf{x}\right)$; for the activation and normalization $\phi\left(\mathbf{Wx}, \mathbf{v}\right) = \frac{\lambda\sigma\left(\mathbf{v}^\top\mathbf{x}+b'\right)}{\|\mathbf{W}h(\mathbf{x})+\mathbf{b}\|}\left(\mathbf{W}h\left(\mathbf{x}\right) + \mathbf{b}\right)$, where σ is the sigmoid function, $\mathbf{b}$ and b' are bias terms, $\lambda > 0$ controls the scaling range, h is the activation function. And then, we need to construct the message graph.

Hyperbolic Dirichlet Energy. Given the hyperbolic embedings $\mathbf{x} = \left\{\mathbf{x}_i \in \mathbb{L}_K^d\right\}_{i=1}^{|\mathcal{V}|}$, the hyperbolic Dirichlet energy (*HDE*) $E_H^K\left(\mathbf{x}\right)$ is defined as

$$E_H^K\left(\mathbf{x}\right) = \frac{1}{2}\sum_{i,j=1}^{N} d_{\mathcal{L}}^K\left(\exp_{\mathbf{o}}^K\frac{log_{\mathbf{o}}^K\left(\mathbf{x}_i\right)}{\sqrt{1+d_i}}, \exp_{\mathbf{o}}^K\frac{log_{\mathbf{o}}^K\left(\mathbf{x}_j\right)}{\sqrt{1+d_j}}\right)^2, \tag{10}$$

where $d_{i/j}$ denotes the node degree of node i/j. The distance $d_{\mathcal{L}}^{K}(\mathbf{x}, \mathbf{y})$ between two points $\mathbf{x}, \mathbf{y} \in \mathbb{L}$ is the geodesic. Given that each node is connected to every other node in videos, resulting in a node degree d_i of $n-1$ (where n is the total number of nodes), the formula for hyperbolic Dirichlet energy can be simplified.

$$E_H^K(\mathbf{x}) = \frac{1}{2} \sum_{i,j=1}^{N} d_{\mathcal{L}}^{K}(\mathbf{x}_i, \mathbf{x}_j)^2 . \tag{11}$$

HDE is used to measure the similarity between node features in order to gauge the degree of information aggregation among features. It is evident that as hyperbolic message aggregation progresses, the similarity between features gradually decreases. Hyperbolic message aggregation reduces *HDE*. It can be expressed as: $E_H^K\left(\mathbf{x}^{(l+1)}\right) \leq E_H^K\left(\mathbf{x}^{(l)}\right)$, where l is the layer number.

Layer-Sensitive Hyperbolic Association Degree. Based on *HDE*, we design *Layer-Sensitive Hyperbolic Association Degree (LSHAD)* to guide the node selection strategy for our construction of graphs for message aggregation. It is defined as

$$LSHAD_k = f\left(E_H^K(x), k\right) = sigmoid(\beta k - \gamma + \frac{1}{E_H^K(x) + 1}), \tag{12}$$

where $f(\cdot)$ is a function related to k and $E_H^K(x)$, k is the current layer number. β and γ are hyperparameters.

Lorentzian similarity. Based on the Lorentzian distance, the Lorentzian similarity to measure the feature semantic similarity between nodes is given by

$$Ls(x_i, x_j) = exp(-d_{\mathcal{L}}^{K}(x_i, x_j)), \tag{13}$$

where $d_{\mathcal{L}}^{K}(\cdot,\cdot)$ is the Lorentzian intrinsic distance function. We define the initial adjacent matrix $A^{\mathbb{L}} \in \mathbb{R}^{T \times T}$ via lorentz similarity:

$$A_{i,j}^{\mathbb{L}} = softmax(Ls(x_i, x_j)). \tag{14}$$

***LSHAD* Construct rules.** With *LSHAD*, we propose message graph construction rules, called *LSHAD* construct rules. It is defined as

$$\begin{cases} A'_{i,j} = A_{i,j}, & \text{if } A_{i,j} \geq LSHAD^k \\ A'_{i,j} = 0, & \text{if } A_{i,j} < LSHAD^k, \end{cases} \tag{15}$$

where $A_{i,j}$ means the lorentz similarity between nodes i and j in the graph G. Formally, it enforces the elements of the adjacency matrix A that are less than *LSHAD* to be zeros. Finally, we can dynamically construct message graphs at each layer via *LSHAD* construct rules to obtain better contextual information. Following *LSHAD* construction rules, we can dynamically construct message graphs G', which we then use to perform message aggregation operations to obtain better contextual information.

Hyperbolic Message Aggregation. We use graph G' to perform message aggregation, and the message aggregation can be defined as:

$$MA(\mathbf{y}_i) = \frac{\sum_{j=1}^{m} A_{ij} \mathbf{y}_j}{\sqrt{-K}\left| \| \sum_{k=1}^{m} A_{ik} \mathbf{y}_k \|_{\mathcal{L}} \right|}, \tag{16}$$

where m is the number of nodes. y_i is the node features.

4.2 Dual-Space Interaction Module

Although hyperbolic representation learning enhances understanding of event hierarchies, visual representations remain crucial in violence detection. Fusing representations from different spaces is challenging; thus, DSI employs cross-space attention to facilitate interactions between Euclidean and hyperbolic spaces.

Cross-Space Attention Mechanism. Cross-Space Attention Mechanism utilizes the Lorentzian metric to calculate attention scores between nodes from different spaces, accurately measuring semantic similarity and better preserving their true relationships by computing the nonlinear distance between them. We denote the features in Euclidean space as V_E and the features in hyperbolic space as V_H. $CSA_{E \to H}$ models the between-graph interaction and guides the transfer of inter-graph message from V_E to V_H. First, we use linear layer to transform V_H to the *key* graph V_k and the *value* graph V_v,and V_E to the *query* graph V_q. Then, we use lorentzian metric to calculate the attention map $\mathcal{A}_{E\to H}$ as follows:

$$\mathcal{A}_{E\to H} = softmax(Ls(V_q, V_k)), Ls(x_i, x_j) = \begin{cases} Ls(x_i, x_j), & \text{if } Ls(x_i, x_j) > \lambda \\ 0, & \text{if } Ls(x_i, x_j) \leq \lambda, \end{cases} \tag{17}$$

where $Ls(\cdot)$ is Lorentzian similarity defined in Eq. 13 and λ is the threshold value to eliminate weak relations and strengthen correlations of more similar pairs. The representation from E to H can be formulated as follows:

$$V'_H = CSA_{E\to H}(V_H, V_E) = softmax(\frac{\mathcal{A}_{E\to H} \times V_k}{\sqrt{d}})V_v. \tag{18}$$

The interaction process in DSI can be represented as follows:

$$\begin{aligned} V'_E &= \alpha \times CSA_{E\to H}(V_E, V_H) + V_E \\ V'_H &= \alpha \times CSA_{H\to E}(V_H, V'_E) + V_H \\ V_F &= MaxPool([V'_E \oplus V'_H]), \end{aligned} \tag{19}$$

where V'_E represents the features obtained by enhancing Euclidean space features using hyperbolic space features, and α controls the contribution of the enhanced features and V_E. $MaxPool$ is the max pooling operation and $\oplus$ represents the concatenation operation.

Learning Objective. We use binary cross-entropy as our classification loss. Its calculation formula is:

$$Loss = -\frac{1}{N}\sum_{i=1}^{N}\left(y_i \log(\hat{y}_i) + (1 - y_i)log(1 - \hat{y}_i)\right), \tag{20}$$

where y_i is true label, $\hat{y}_i$ is the predicted label, N is the batch size.

5 Experiments

5.1 Experiments Setup

Datasets. Under the multimodal input setting, we follow [34, 37, 25] to conduct experiments on XD-Violence, which is the only and extremely challenging VVD dataset with multimodal information. Under the unimodal input setting, both the XD-Violence[34] and UCF-Crime[30] datasets are used to evaluate our method. More details of the two dataset settings are provided in the Appendix.

Evaluation Metrics. To quantitatively evaluate the performance, we follow standard pratice [34, 37, 18, 6]. For XD-Violence, we utilize the frame-level average precision (AP) as the evaluation metric. For UCF-Crime, we adopt the area under the curve of the frame-level receiver operating characteristic (AUC) to evaluate performance.

5.2 Comparisons with State-of-the-art Methods

In Table 1, with multimodal input, our DSRL demonstrates superior performance on XD-Violence, surpassing the best method that uses Euclidean space representation by 4.21% and that uses only hyperbolic space representation by 1.94%. These results highlight the effectiveness of DSRL in learning discriminative features and prove that our dual-space representation learning integrates the benefits of Euclidean and hyperbolic space well. From Table 1, it also can be found that DSRL achieves SOTA performance under unimodal input settings on XD-Violence, outperforming existing state-of-the-art methods. Furthermore, to analyse the generalization of our method, we also report the performance on the UCF-Crime dataset, achieving an accuracy of 86.38%, comparable to current state-of-the-art methods.

5.3 Ablation Studies

We conduct ablation studies on various design choices of our DSRL to demonstrate their contributions to the final results in Table 2.

Table 1: Comparisons of frame-level AP performance on XD-Violence and AUC performance on UCF-Crime datasets under different input settings. UCF-Crime only has visual modality input.

Methods	Input Setting	Feature Space	UCF-Crime	XD-Violence
Sultani et al. [30]	Unimodal	Euclidean	76.21	73.20
Wu et al. [33]	Unimodal	Euclidean	82.44	75.90
RTFM [31]	Unimodal	Euclidean	84.30	77.81
MSL [16]	Unimodal	Euclidean	85.30	78.28
MGFN [6]	Unimodal	Euclidean	**86.98**(1^{st})	79.19(3^{rd})
UMIL [18]	Unimodal	Euclidean	86.75(2^{nd})	81.66(2^{nd})
CU-Net [39]	Unimodal	Euclidean	86.22	78.74
Ours	Unimodal	Euclidean and Hyperbolic	86.38(3^{rd})	**82.01**(1^{st})
HL-Net [34]	Multimodal	Euclidean	-	78.64
Wu et al. [35]	Multimodal	Euclidean	-	78.64
Pang et al. [23]	Multimodal	Euclidean	-	79.37
UMIL [18]	Multimodal	Euclidean	-	81.77
Zhang et al. [39]	Multimodal	Euclidean	-	81.43
MACIL-SD [37]	Multimodal	Euclidean	-	83.40(3^{rd})
HyperVD [25]	Multimodal	Hyperbolic	-	85.67(2^{nd})
Ours	Multimodal	Euclidean and Hyperbolic	-	**87.61**(1^{st})

Table 2: Ablations on XD-Violence dataset.

Euclidean	Hyperbolic		DSI			XD-Violence	
GCN	HE-GCN	HGCN	Concat	Cosine Metric	Lorentzian Metric	Multimodal(%)	Unimodal(%)
✓						84.04	77.95
✓		✓	✓			85.01	77.93
✓	✓		✓			86.46	79.70
✓	✓			✓		86.91	80.72
✓	✓				✓	87.61	82.01

1) **Component-wise ablations.** To study the impact of each component in the DSRL, including HE-GCN and DSI, we start with a baseline model that only applies GCN and progressively adds each component. Table 2 shows that the baseline yields inferior performance due to learning representations only in Euclidean space (1^{st} row). Then, HE-GCN is employed and the representations from different spaces are simply concat at this stage, benefit from the hierarchical context of events, resulting in an improvement of 2.42% on multimodal setting and 1.75% on unimodal setting respectively (3^{rd} row). Then DSI is introduced to facilitate information interactions, which further enhances the performance on multimodal input setting by 1.15% and unimodal input setting by 2.31% (5^{th} row). 2) **Effect of *LSHAD*.** *LSHAD* is a crucial element of our HE-GCN for constructing the message graph. In Table 2(2^{nd} and 3^{rd} rows), we present experiments comparing HGCN used in HyperVD [25], which employs a hard node selection strategy (nodes selected by a fixed threshold), with HE-GCN, which uses our introduced layer-sensitive hyperbolic association degrees for node selection in message aggregation. The performance of AP improved by 1.45% in the multimodal setting and by 1.77% on the unimodal setting. These results demonstrate that our *LSHAD* is a better strategy and helps to capture the hierarchical context of events. 3) **Lorentzian metric in DSI.** As shown in Table 2(4^{th} and 5^{th} rows), we also explore the effect of cosine similarity and Lorentzian metric in our DSI, and the results show that using cosine similarity to calculate the attention between nodes resulted in a 0.7% lower performance compared with using the Lorentzian metric. This indicates that the Lorentzian metric is more effective in measuring feature similarity across different spaces.

5.4 Qualitative Results

1) **Feature Discrimination Visualization.** We present t-SNE visualizations of feature distributions on the XD-Violence test set. As shown in Figure 3, red dots represent violent features, while purple dots represent normal features. The clear clustering of violent and non-violent features demonstrates the effectiveness of DSRL.
2) **Qualitative Visualizations.** We illustrate the qualitative visualizations of VVD for the test video

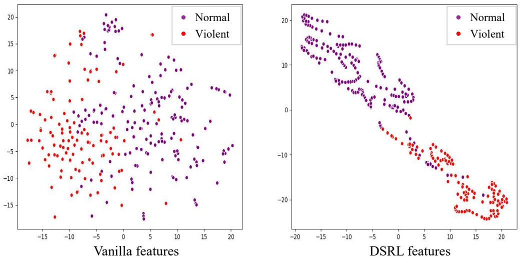

Figure 3: t-SNE visualization of vanilla and DSRL features for the test video on XD-Violence.

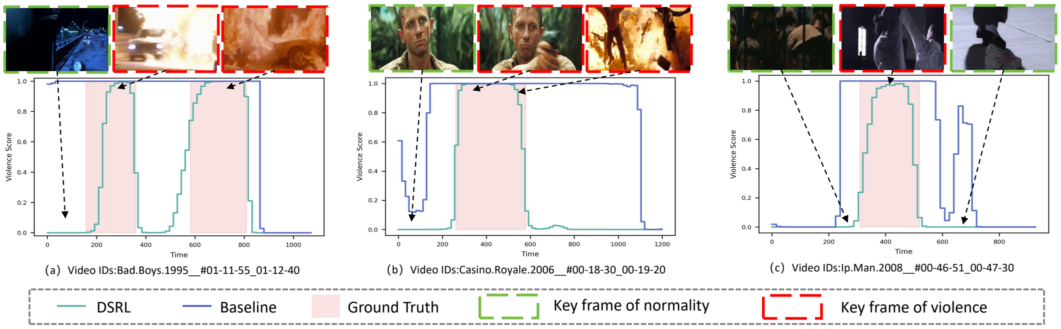

(a) Video IDs:Bad.Boys.1995__#01-11-55_01-12-40

(b) Video IDs:Casino.Royale.2006__#00-18-30_00-19-20

(c) Video IDs:Ip.Man.2008__#00-46-51_00-47-30

Figure 4: Frame-level scores and violence localization examples for the test video from XD-Violence dataset.

from the XD-Violence dataset. Figure 4 shows that DSRL can accurately detect violent events and has a better detection performance than the baseline.

3) **Qualitative Visualizations of DSRL in the Context of Ambiguous Violence.** We put up qualitative visualizations of DSRL when handling ambiguous violence. Figure 5 demonstrates that DSRL effectively resolves ambiguous violence, which single-space representation learning struggles with. In Figure 5(a), the first frame shows smoke caused by fire. Euclidean space representation, relying on visual features, misidentifies the smoke as violence. Hyperbolic space representation, considering contextual information, also misidentifies it due to preceding violent frames. DSRL, however, combines both perspectives: Euclidean space flags the smoke as a potential violence indicator, while hyperbolic space recognizes the fire context. This integration allows DSRL to accurately classify the smoke as non-violent. This supports our motivation: hyperbolic representation enhances hierarchical event relations but weakens visual feature expression, while Euclidean representation emphasizes visual features but overlooks event relationships. DSRL effectively addresses ambiguous violence, which is challenging for either space alone. More performance visualizations are included in the Appendix.

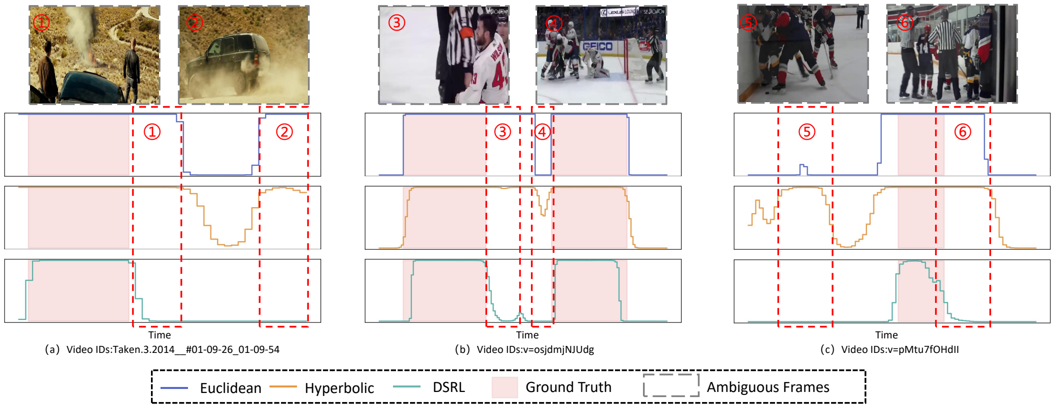

(a) Video IDs:Taken.3.2014__#01-09-26_01-09-54

(b) Video IDs:v=osjdmjNJUdg

(c) Video IDs:v=pMtu7fOHdIl

Figure 5: Some visual results of DSRL in the context of ambiguous violence. "Euclidean" represents the results of GCN only. "Hyperbolic" refers to the results of HyperVD.

5.5 Comparisons of Computing Resources and Training Time

Our designs, HE-GCN and DSI, are specifically crafted to effectively capture hierarchical contextual information of events and to integrate two distinct spaces of information, respectively. To evaluate the benefits of these designs, we conducted experiments on the XD-Violence dataset, training three models for 30 epochs each on a single NVIDIA RTX A6000 GPU: the Baseline (GCN), Baseline+HE-GCN, and Baseline+HE-GCN+DSI (referred to as DSRL). As shown in Table 3, our DSRL model demonstrated a 3.57% improvement in Average Precision (AP) compared to the Baseline. Additionally, the training time per epoch increased by only 41 seconds, and memory usage rose by just 4.1 GB. Both increases are within a reasonable range, making the performance gains achieved by DSRL well worth the additional resource consumption.

Table 3: Comparison of computing resources and training time.

Methods	Params	Training time per epoch	Training time	Video memory usage	AP (%)
Baseline(GCN)	0.7734M	2min	60min	4.24GB	84.04
Baseline+HE-GCN	0.8975M	2min19s	69min39s	7.03GB	86.46
Baseline+HE-GCN+DSI(DSRL)	0.9966M	2min41s	80min19s	8.34GB	87.61

5.6 Analysis of Model Computational Complexity and Speed

The computational efficiency of the DSRL model is crucial, especially for real-time applications. Our analysis confirms that the model meets the requirements for real-time processing, as demonstrated by the following results. Our experiments were conducted on a single NVIDIA RTX A6000 GPU. For **video input**, the model processes at a rate of 83.87 FPS, handling only video data. The model's parameters are relatively lightweight, totaling 13.4 MB, with I3D parameters at 12.49 MB and DSRL parameters at 0.91 MB. This compact size ensures quick response times. When processing **video and audio inputs**, the model maintains a high processing speed of 56.86 FPS, despite the added computational load from audio processing. The total parameter size for this configuration is 85.54 MB, comprising I3D parameters at 12.49 MB, VGGish parameters at 72.14 MB, and DSRL parameters at 0.91 MB. These results illustrate that our model exhibits excellent real-time performance, even with multimodal inputs, making it suitable for latency-sensitive real-world applications.

6 Conclusions

In this paper, we propose a comprehensive geometric representation learning method, Dual-Space Representation Learning (DSRL) which integrates the benefits of Euclidean and hyperbolic geometries to improve the discrimination of ambiguous violence. Hyperbolic Energy-constrained Graph Convolutional Network (HE-GCN) is designed to better capture the hierarchical context of events. Additionally, Dual-Space Interaction (DSI) is designed to facilitate information interactions. Our method achieves SOTA performance on the XD-Violence dataset in both unimodal and multimodal settings, especially excelling in resolving ambiguous violence.

Limitions. Our DSRL is effective for VVD in a multimodal input setting. However, DSRL only utilizes basic audio information, potentially overlooking the more detailed semantic content present in the audio. How to further narrow this limitation is our future research focus. Due to the bias issues in the XD-Violence and UCF-Crime datasets, which fail to adequately represent diverse backgrounds, the fairness and generalization of the model may be affected. In the future, we hope to use more diverse datasets and conduct bias analysis to prevent the model from producing unfair outcomes due to false associations with gender or race.

Acknowledgements. This work was supported in part by the Science and Technology Innovation Key R&D Program of Chongqing under Grant No. CSTB2023TIAD-STX0016, in part by the National Natural Science Foundation of China under Grants No. 62472060, 62441601, U23A20318, and 62221005, in part by the Natural Science Foundation of Chongqing under Grand No. CSTB2022NSCQ-MSX1024, CSTB2023NSCQ-LZX0061, in part by the Science and Technology Research Program of Chongqing Municipal Education Commission under Grant No. KJZD-K202300604, and in part by the Chongqing Institute for Brain and Intelligence.

References

[1] Mina Ghadimi Atigh, Julian Schoep, Erman Acar, Nanne Van Noord, and Pascal Mettes. Hyperbolic image segmentation. In *Proceedings of the IEEE/CVF conference on computer vision and pattern recognition*, pages 4453–4462, 2022.

[2] Joao Carreira and Andrew Zisserman. Quo vadis, action recognition? a new model and the kinetics dataset. In *proceedings of the IEEE Conference on Computer Vision and Pattern Recognition*, pages 6299–6308, 2017.

[3] Ines Chami, Zhitao Ying, Christopher Ré, and Jure Leskovec. Hyperbolic graph convolutional neural networks. *Advances in neural information processing systems*, 32, 2019.

[4] Lin Chen. Topological structure in visual perception. *Science*, 218(4573):699–700, 1982.

[5] Weize Chen, Xu Han, Yankai Lin, Hexu Zhao, Zhiyuan Liu, Peng Li, Maosong Sun, and Jie Zhou. Fully hyperbolic neural networks. *arXiv preprint arXiv:2105.14686*, 2021.

[6] Yingxian Chen, Zhengzhe Liu, Baoheng Zhang, Wilton Fok, Xiaojuan Qi, and Yik-Chung Wu. Mgfn: Magnitude-contrastive glance-and-focus network for weakly-supervised video anomaly detection. In *Proceedings of the AAAI Conference on Artificial Intelligence*, volume 37, pages 387–395, 2023.

[7] Jia-Chang Feng, Fa-Ting Hong, and Wei-Shi Zheng. Mist: Multiple instance self-training framework for video anomaly detection. In *Proceedings of the IEEE/CVF conference on computer vision and pattern recognition*, pages 14009–14018, 2021.

[8] Yuan Gao, Hong Liu, Xiaohu Sun, Can Wang, and Yi Liu. Violence detection using oriented violent flows. *Image and vision computing*, 48:37–41, 2016.

[9] Songwei Ge, Shlok Mishra, Simon Kornblith, Chun-Liang Li, and David Jacobs. Hyperbolic contrastive learning for visual representations beyond objects. In *Proceedings of the IEEE/CVF Conference on Computer Vision and Pattern Recognition*, pages 6840–6849, 2023.

[10] Tal Hassner, Yossi Itcher, and Orit Kliper-Gross. Violent flows: Real-time detection of violent crowd behavior. In *2012 IEEE computer society conference on computer vision and pattern recognition workshops*, pages 1–6. IEEE, 2012.

[11] Shawn Hershey, Sourish Chaudhuri, Daniel PW Ellis, Jort F Gemmeke, Aren Jansen, R Channing Moore, Manoj Plakal, Devin Platt, Rif A Saurous, Bryan Seybold, et al. Cnn architectures for large-scale audio classification. In *2017 ieee international conference on acoustics, speech and signal processing (icassp)*, pages 131–135. IEEE, 2017.

[12] Jie Hong, Pengfei Fang, Weihao Li, Junlin Han, Lars Petersson, and Mehrtash Harandi. Curved geometric networks for visual anomaly recognition. *IEEE Transactions on Neural Networks and Learning Systems*, 2023.

[13] Gao Huang, Yixuan Li, Geoff Pleiss, Zhuang Liu, John E Hopcroft, and Kilian Q Weinberger. Snapshot ensembles: Train 1, get m for free. *arXiv preprint arXiv:1704.00109*, 2017.

[14] Diederik P Kingma and Jimmy Ba. Adam: A method for stochastic optimization. *arXiv preprint arXiv:1412.6980*, 2014.

[15] Shuang Li, Fan Li, Jinxing Li, Huafeng Li, Bob Zhang, Dapeng Tao, and Xinbo Gao. Logical relation inference and multiview information interaction for domain adaptation person re-identification. *IEEE Transactions on Neural Networks and Learning Systems*, 2023.

[16] Shuo Li, Fang Liu, and Licheng Jiao. Self-training multi-sequence learning with transformer for weakly supervised video anomaly detection. In *Proceedings of the AAAI Conference on Artificial Intelligence*, volume 36, pages 1395–1403, 2022.

[17] Teng Long, Pascal Mettes, Heng Tao Shen, and Cees GM Snoek. Searching for actions on the hyperbole. In *Proceedings of the IEEE/CVF Conference on Computer Vision and Pattern Recognition*, pages 1141–1150, 2020.

[18] Hui Lv, Zhongqi Yue, Qianru Sun, Bin Luo, Zhen Cui, and Hanwang Zhang. Unbiased multiple instance learning for weakly supervised video anomaly detection. In *Proceedings of the IEEE/CVF conference on computer vision and pattern recognition*, pages 8022–8031, 2023.

[19] Oded Maron and Tomás Lozano-Pérez. A framework for multiple-instance learning. *Advances in neural information processing systems*, 10, 1997.

[20] Sadegh Mohammadi, Alessandro Perina, Hamed Kiani, and Vittorio Murino. Angry crowds: Detecting violent events in videos. In *Computer Vision–ECCV 2016: 14th European Conference, Amsterdam, The Netherlands, October 11–14, 2016, Proceedings, Part VII 14*, pages 3–18. Springer, 2016.

[21] Maximillian Nickel and Douwe Kiela. Learning continuous hierarchies in the lorentz model of hyperbolic geometry. In *International conference on machine learning*, pages 3779–3788. PMLR, 2018.

[22] Wen-Feng Pang, Qian-Hua He, Yong-jian Hu, and Yan-Xiong Li. Violence detection in videos based on fusing visual and audio information. In *ICASSP 2021-2021 IEEE international conference on acoustics, speech and signal processing (ICASSP)*, pages 2260–2264. IEEE, 2021.

[23] Wenfeng Pang, Wei Xie, Qianhua He, Yanxiong Li, and Jichen Yang. Audiovisual dependency attention for violence detection in videos. *IEEE Transactions on Multimedia*, 2022.

[24] Wei Peng, Jingang Shi, Zhaoqiang Xia, and Guoying Zhao. Mix dimension in poincaré geometry for 3d skeleton-based action recognition. In *Proceedings of the 28th ACM International Conference on Multimedia*, pages 1432–1440, 2020.

[25] Xiaogang Peng, Hao Wen, Yikai Luo, Xiao Zhou, Keyang Yu, Yigang Wang, and Zizhao Wu. Learning weakly supervised audio-visual violence detection in hyperbolic space. *arXiv preprint arXiv:2305.18797*, 2023.

[26] Fernando J Rendón-Segador, Juan A Álvarez-García, Jose L Salazar-González, and Tatiana Tommasi. Crimenet: Neural structured learning using vision transformer for violence detection. *Neural networks*, 161:318–329, 2023.

[27] Jiangming Shi, Xiangbo Yin, Yeyun Chen, Yachao Zhang, Zhizhong Zhang, Yuan Xie, and Yanyun Qu. Multi-memory matching for unsupervised visible-infrared person re-identification. In *ECCV*, page 456–474, 2024.

[28] Jiangming Shi, Yachao Zhang, Xiangbo Yin, Yuan Xie, Zhizhong Zhang, Jianping Fan, Zhongchao Shi, and Yanyun Qu. Dual pseudo-labels interactive self-training for semi-supervised visible-infrared person re-identification. In *ICCV*, pages 11218–11228, 2023.

[29] Swathikiran Sudhakaran and Oswald Lanz. Learning to detect violent videos using convolutional long short-term memory. In *2017 14th IEEE international conference on advanced video and signal based surveillance (AVSS)*, pages 1–6. IEEE, 2017.

[30] Waqas Sultani, Chen Chen, and Mubarak Shah. Real-world anomaly detection in surveillance videos. In *Proceedings of the IEEE conference on computer vision and pattern recognition*, pages 6479–6488, 2018.

[31] Yu Tian, Guansong Pang, Yuanhong Chen, Rajvinder Singh, Johan W Verjans, and Gustavo Carneiro. Weakly-supervised video anomaly detection with robust temporal feature magnitude learning. In *Proceedings of the IEEE/CVF international conference on computer vision*, pages 4975–4986, 2021.

[32] Yiming Wang, Guanqiu Qi, Shuang Li, Yi Chai, and Huafeng Li. Body part-level domain alignment for domain-adaptive person re-identification with transformer framework. *IEEE Transactions on Information Forensics and Security*, 17:3321–3334, 2022.

[33] Peng Wu and Jing Liu. Learning causal temporal relation and feature discrimination for anomaly detection. *IEEE Transactions on Image Processing*, 30:3513–3527, 2021.

[34] Peng Wu, Jing Liu, Yujia Shi, Yujia Sun, Fangtao Shao, Zhaoyang Wu, and Zhiwei Yang. Not only look, but also listen: Learning multimodal violence detection under weak supervision. In *Computer Vision–ECCV 2020: 16th European Conference, Glasgow, UK, August 23–28, 2020, Proceedings, Part XXX 16*, pages 322–339. Springer, 2020.

[35] Peng Wu, Xiaotao Liu, and Jing Liu. Weakly supervised audio-visual violence detection. *IEEE Transactions on Multimedia*, 25:1674–1685, 2023.

[36] Long Xu, Chen Gong, Jie Yang, Qiang Wu, and Lixiu Yao. Violent video detection based on mosift feature and sparse coding. In *2014 IEEE International Conference on Acoustics, Speech and Signal Processing (ICASSP)*, pages 3538–3542. IEEE, 2014.

[37] Jiashuo Yu, Jinyu Liu, Ying Cheng, Rui Feng, and Yuejie Zhang. Modality-aware contrastive instance learning with self-distillation for weakly-supervised audio-visual violence detection. In *Proceedings of the 30th ACM International Conference on Multimedia*, pages 6278–6287, 2022.

[38] Zhen Yu, Toan Nguyen, Yaniv Gal, Lie Ju, Shekhar S Chandra, Lei Zhang, Paul Bonnington, Victoria Mar, Zhiyong Wang, and Zongyuan Ge. Skin lesion recognition with class-hierarchy regularized hyperbolic embeddings. In *International Conference on Medical Image Computing and Computer-Assisted Intervention*, pages 594–603. Springer, 2022.

[39] Chen Zhang, Guorong Li, Yuankai Qi, Shuhui Wang, Laiyun Qing, Qingming Huang, and Ming-Hsuan Yang. Exploiting completeness and uncertainty of pseudo labels for weakly supervised video anomaly detection. In *Proceedings of the IEEE/CVF Conference on Computer Vision and Pattern Recognition*, pages 16271–16280, 2023.

Appendix

Here we provide the proof of Theorem 1 in Sec. A. The Technical details of the DSRL are introduced in Sec. B. Moreover, the datasets settings and implementation details are shown in Sec. C. We conduct additional experiments in Sec. D, and more qualitative results in Sec. E. Broader impacts are listed in Sec.F.

A Proof of Theorem. 1

Theorem 1. $\forall \mathbf{x} \in \mathbb{L}^n$, $\mathbf{M} \in \mathbb{R}^{(m+1)\times(n+1)}$, we have $f_x(\mathbf{M})\mathbf{x} \in \mathbb{L}^m_K$.

Proof 1.

$$\mathbf{y} = f_{\mathbf{x}}(\mathbf{M})\mathbf{x} = \begin{bmatrix} \frac{\sqrt{\|W\mathbf{x}\|^2 - 1/K}}{\mathbf{v}^\top \mathbf{x}} \mathbf{v}^\top \mathbf{x} \\ \mathbf{W}\mathbf{x} \end{bmatrix} = \begin{bmatrix} \sqrt{\|W\mathbf{x}\|^2 - 1/K} \\ \mathbf{W}\mathbf{x} \end{bmatrix}$$

$$\begin{aligned} \langle \mathbf{y}, \mathbf{y} \rangle_{\mathcal{L}} &= -(\|W\mathbf{x}\|^2 - 1/K) + (\mathbf{W}\mathbf{x})^\top \mathbf{W}\mathbf{x} \\ &= \frac{1}{K} - \|W\mathbf{x}\|^2 + \|W\mathbf{x}\|^2 \\ &= \frac{1}{K} \end{aligned}$$

Thus, $f_x(\mathbf{M})\mathbf{x}$ lies on the manifold $\mathcal{L}$ of the Lorentz model.

B Technical details of the DSRL

As depicted in Figure 2, the entire process can be divided into feature preprocessing to integrate the features of the two modalities; representation learning in hyperbolic space to learn the hierarchical context of events; representation learning in Euclidean space to learn the visual features of events; interaction between the two spaces to promote cross-space enhancement; and finally, feeding the features into a hyperbolic classifier for classification.

Feature Preprocessing. Following the previous works[34, 23], the visual and audio segments are processed by the I3D [2] network pretrained on the Kinetics-400 dataset and the VGGish[11] network pretrained on a large YouTube dataset, respectively. After that, we perform further feature extraction using simple convolution and pooling operations. A simple cross-modal attention mechanism is then employed to enhance the audio features, which are subsequently concatenated with the visual features to form the fused features.

Hyperbolic Representation Learning. In this part, we first use HE-GCN to learn the hierarchical context of events. Meanwhile, the temporal relation is also crucial for numerous video-based tasks. Therefore, we construct a temporal relation graph directly based on the temporal structure of a video and learn the temporal relation among snippets in hyperbolic space via HGCN. Its adjacency matrix $A^{\mathbb{T}} \in \mathbb{R}^{T\times T}$ is only dependent on temporal positions of the i-th and j-th snippets, which can be defined as:

$$A^{\mathbb{T}}_{ij} = exp(-\frac{|i-j|}{\sigma}) \tag{21}$$

where σ controls the range of influence of distance relation. Finally, we use HE-GCN for semantic message aggregation and HGCN for temporal message aggregation, then concatenate them to obtain a hyperbolic space representation.

Euclidean Representation learning. The process of representation learning in Euclidean space is similar to that in hyperbolic space and follows a dual-branch structure, considering both semantic and temporal relationships. We use cosine similarity to compute the semantic similarity in Euclidean space and use Eq. 21 to compute temporal relationships. Finally, we employ GCN for message aggregation and concatenate them to obtain the final representation in Euclidean space.

Dual-Space Interaction. In this part, we primarily use cross-space attention to enhance the interaction between the features of the two spaces. The detailed process is described in Sec. 4.2.

Hyperbolic Classifier. As shown in Figure.2, we input the enhanced embeddings from DSI into hyperbolic classifier utilizing Lorentzian metric, which can be formalized as:

$$S = \sigma(\epsilon + \epsilon \left\langle F, W \right\rangle_{\mathcal{L}} + b) \tag{22}$$

where σ is sigmoid function and W is weight matrices. b and ϵ denotes bias term and hyper-parameter, respectively. Lastly, we supervise the training of the violence scores obtained by the model with the real labels using the binary cross-entropy loss.

C Experimental Details

Dataset. We conducted experiments on XD-Violence with both multi-modal input settings and single-modal input settings. Additionally, we performed experiments on UCF-Crime with single-modal input settings to demonstrate the generalization capability of DSRL.
1) **XD-Violence** dataset is by far the only available large-scale audio-visual dataset for violence detection, which is also the largest dataset compared with other unimodal datasets. XD-Violence consists of 4,757 untrimmed videos (217 hours) and six types of violent events, which are curated from real-life movies and in-the-wild scenes on YouTube. For XD-Violence dataset, only video-level annotations are provided.
2) **UCF-Crime** dataset is a large-scale dataset comprised of real-world videos captured by surveillance cameras. It consists of 1,610 training videos annotated with video-level labels and 290 test videos annotated at the frame level to facilitate performance evaluation. The videos are collected from different scenes and encompass 13 distinct categories of anomalies.
Implementation Details. The visual sample rate is set to 24 fps, and visual features are extracted by a sliding window with a size of 16 frames. For the audio data, we first divide each audio into 960-ms overlapped segments and compute the log-mel spectrogram with 96 × 64 bins. Our proposed method is trained for 30 epochs in total, and the batch size is 256. The initial learning rate is 0.001, which is dynamically adjusted by a cosine annealing scheduler [13]. We use Adam [14] as the optimizer without weight decay. For hyper-parameters, we set β as 0.8, γ as 1.2, α as 0.3, and dropout rate as 0.6. Following [25], σ is empirically set to e. For the MIL, we set the value k of k-max activation as $\left\lfloor \frac{T}{16} + 1 \right\rfloor$, where T denotes the length of the input feature.
Experiments Compute Resources. We use an Intel(R) Xeon(R) Platinum 8260 CPU @ 2.40GHz, a NVIDIA RTX A6000 GPU to conduct experiments. We use CUDA 12.2, Python 3.9.16, and Pytorch 1.12.1.

D Additional Experiments

Reasons for the design choices in LSHAD with its multiple hyperparameters and threshold criteria.
Inspired by the Global-first principle[4] that humans always have cognition on global first and then focus on local, we propose a novel node selection strategy, which guarantees the model captures the broader global context first with a relaxed threshold at the beginning of message aggregation and then focuses on the local context with more strict thresholds. To achieve this, we introduce the LSHAD construction rule, which calculates an LSHAD threshold based on the number of the current layer K and hyperbolic Dirichlet energy of the current layer. As the K increases and the hyperbolic Dirichlet energy decreases, the LSHAD threshold increases and is limited to 0 and 1 by the sigmoid function. If there is no β and γ, the threshold in the first layer will be strict (> 0.5), causing the overlook of some global context information. Therefore, to make our node selection threshold conform to the Global-first principle, we introduced the two hyperparameters in LSHAD, where β controls the influence of the number of current layer k and γ acts as a bias to fine-tune the threshold. Moreover, we conducted an ablation study to determine the optimal value of the two hyperparameters (β,γ), where β ranges from [0.2,0.4,0.6,0.8,1.0] and γ ranges from [1.0,1.2,1.4,1.6,1.8,2.0]. The results in the table below reveal that when $\gamma - \beta$ is 0.4, the performance is optimal, so we chose a pair (0.8, 1.2) from this set.
Ablation studies on some hyperparameters in DSI.
Moreover, we conduct ablation studies on some hyperparameters in DSI. Table 5 and 6 show the experimental results.

Table 4: Ablation studies on β and γ.

β \ γ	1.0	1.2	1.4	1.6	1.8	2.0
0.2	85.22	87.12	86.32	86.60	86.31	86.86
0.4	87.52	85.22	87.12	86.32	86.60	86.31
0.6	87.61	87.52	85.22	87.12	86.32	86.60
0.8	87.29	87.61	87.52	85.22	87.12	86.32
1.0	86.29	87.29	87.61	87.52	85.22	87.12

Table 5: Ablation studies on λ of DSI.

λ	0.1	0.2	0.3	0.4	0.5	0.6	0.7	0.8	0.9
AV-AP	87.14	87.38	87.1	87.32	86.53	87.2	87.4	87.61	87.23

Table 6: Ablation studies on α of DSI.

α	0.1	0.2	0.3	0.4	0.5	0.6	0.7	0.8	0.9
AV-AP	87.18	87.16	87.61	87.21	87.26	86.91	87.42	86.59	87.51

E Visualization

Inference visualizations of the ablation modules.
In this section, we have supplemented inference visualization results for the ablation module, and conducted corresponding visualisation experiments to explore the discriminative power of the model w/ or w/o our core modules, HE-GCN and DSI. We conducted the analysis from two dimensions (the feature-level and the frame-leve), and the results are shown in Figure 6 and Figure 7.
At the feature-level, the results are shown in Figure 6. Compared to GCN, HE-GCN can capture the hierarchical context of events, effectively separating features. This results in a greater distance between feature clusters compared to Figure 6(a) original features and Figure 6(b) using only Euclidean representation learning. However, some challenging feature points remain difficult to distinguish. The addition of the DSI module facilitates information interactions between Euclidean and hyperbolic spaces, capturing more discriminative features to better differentiate these challenging feature points. As shown in Figure 6(d), the DSI module further enhances feature differentiation by effectively combining information from both spaces.

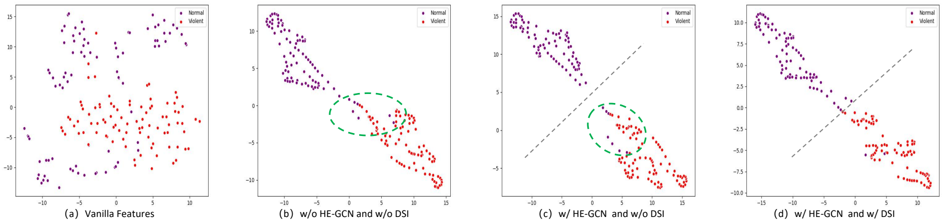

(a) Vanilla Features (b) w/o HE-GCN and w/o DSI (c) w/ HE-GCN and w/o DSI (d) w/ HE-GCN and w/ DSI

Figure 6: t-SNE visualization of the ablation module at feature-level.

Meanwhile, **at the frame-level**, experiments conducted on two test videos as shown in Figure 7 demonstrate that our method significantly improves the discriminative power for identifying violent frames compared to the baseline, which uses only GCN. Compared with the model w/o our core modules, both HE-GCN and DSI contribute to detecting violent frames.

Moreover, we provide more qualitative results, including the qualitative visualizations of VVD (Figure 8) and the qualitative visualizations of DSRL in the context of ambiguous violence (Figure 9).

Qualitative visualizations.
Figure 8 illustrates that DSRL can accurately distinguish between violent and normal events, demonstrating the effectiveness of DSRL. Additionally, compared with the baseline curves, our method shows better performance, further validating the effectiveness of the modules we designed.

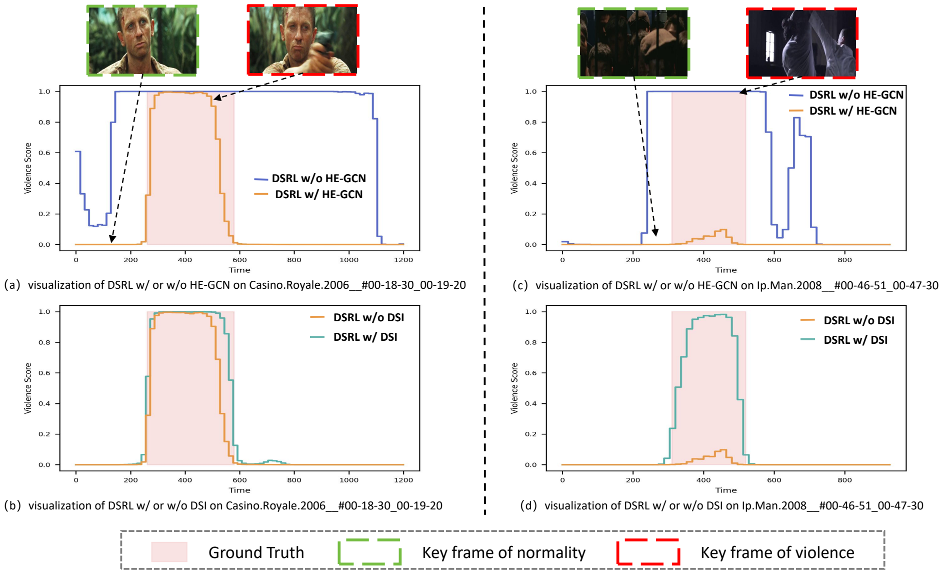

(a) visualization of DSRL w/ or w/o HE-GCN on Casino.Royale.2006__#00-18-30_00-19-20

(c) visualization of DSRL w/ or w/o HE-GCN on Ip.Man.2008__#00-46-51_00-47-30

(b) visualization of DSRL w/ or w/o DSI on Casino.Royale.2006__#00-18-30_00-19-20

(d) visualization of DSRL w/ or w/o DSI on Ip.Man.2008__#00-46-51_00-47-30

Figure 7: Qualitative results of DSRL w/ or w/o our core modules (HE-GCN and DSI) for the test video from XD-Violence dataset at frame-level.

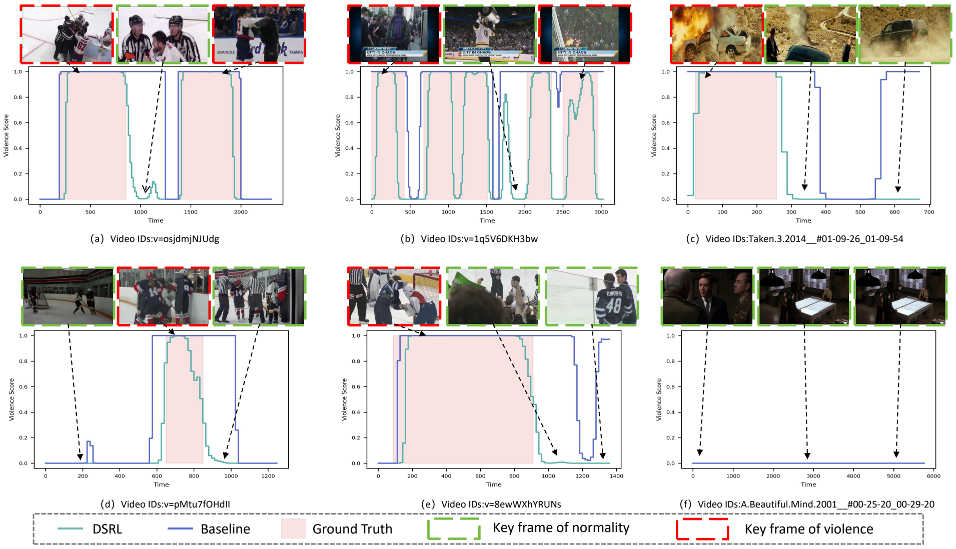

(a) Video IDs:v=osjdmjNJUdg

(b) Video IDs:v=1q5V6DKH3bw

(c) Video IDs:Taken.3.2014__#01-09-26_01-09-54

(d) Video IDs:v=pMtu7fOHdIl

(e) Video IDs:v=8ewWXhYRUNs

(f) Video IDs:A.Beautiful.Mind.2001__#00-25-20_00-29-20

Figure 8: Frame-level scores and violence localization examples for the test video from XD-Violence dataset.

Qualitative Visualizations of DSRL in the context of ambiguous violence.
Figure9 shows that in the XD-Violence test set, DSRL accurately detects the correct categories of ambiguous violence, while using only Euclidean space or only hyperbolic space fails to correctly detect these instances.

F Broader impacts

Potential positive societal impacts.
Our work can be more effective in identifying incidents of violence, albeit it may be ambiguous. This contributes to a higher level of safety in the community and the public's sense of security.
Potential negative societal impacts.
If our algorithm were to be widely applied in monitoring and law enforcement domains, it could

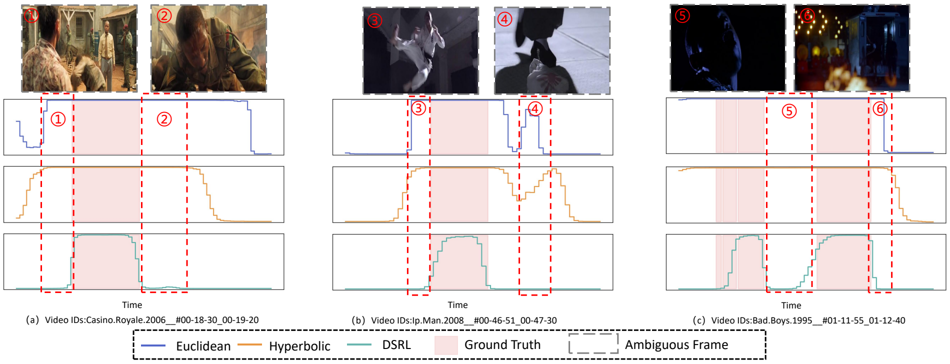

(a) Video IDs:Casino.Royale.2006__#00-18-30_00-19-20

(b) Video IDs:Ip.Man.2008__#00-46-51_00-47-30

(c) Video IDs:Bad.Boys.1995__#01-11-55_01-12-40

Figure 9: Qualitative Visualizations of DSRL in the context of ambiguous violence. The blue curves show violence scores predicted using only Euclidean representation, the yellow curve shows scores using only hyperbolic representation, the green curves show scores predicted by DSRL, and the pink area represents the ground-truth violent temporal location.

exacerbate societal surveillance and control, triggering concerns among the public regarding individual freedom and privacy rights.

NeurIPS Paper Checklist

1. **Claims**

   Question: Do the main claims made in the abstract and introduction accurately reflect the paper's contributions and scope?

   Answer: [Yes]

   Justification: The abstract and introduction clearly state the main claims and contributions of the paper.

   Guidelines:

   - The answer NA means that the abstract and introduction do not include the claims made in the paper.
   - The abstract and/or introduction should clearly state the claims made, including the contributions made in the paper and important assumptions and limitations. A No or NA answer to this question will not be perceived well by the reviewers.
   - The claims made should match theoretical and experimental results, and reflect how much the results can be expected to generalize to other settings.
   - It is fine to include aspirational goals as motivation as long as it is clear that these goals are not attained by the paper.

2. **Limitations**

   Question: Does the paper discuss the limitations of the work performed by the authors?

   Answer: [Yes]

   Justification: Please see Sec.6.

   Guidelines:

   - The answer NA means that the paper has no limitation while the answer No means that the paper has limitations, but those are not discussed in the paper.
   - The authors are encouraged to create a separate "Limitations" section in their paper.
   - The paper should point out any strong assumptions and how robust the results are to violations of these assumptions (e.g., independence assumptions, noiseless settings, model well-specification, asymptotic approximations only holding locally). The authors should reflect on how these assumptions might be violated in practice and what the implications would be.
   - The authors should reflect on the scope of the claims made, e.g., if the approach was only tested on a few datasets or with a few runs. In general, empirical results often depend on implicit assumptions, which should be articulated.
   - The authors should reflect on the factors that influence the performance of the approach. For example, a facial recognition algorithm may perform poorly when image resolution is low or images are taken in low lighting. Or a speech-to-text system might not be used reliably to provide closed captions for online lectures because it fails to handle technical jargon.
   - The authors should discuss the computational efficiency of the proposed algorithms and how they scale with dataset size.
   - If applicable, the authors should discuss possible limitations of their approach to address problems of privacy and fairness.
   - While the authors might fear that complete honesty about limitations might be used by reviewers as grounds for rejection, a worse outcome might be that reviewers discover limitations that aren't acknowledged in the paper. The authors should use their best judgment and recognize that individual actions in favor of transparency play an important role in developing norms that preserve the integrity of the community. Reviewers will be specifically instructed to not penalize honesty concerning limitations.

3. **Theory Assumptions and Proofs**

   Question: For each theoretical result, does the paper provide the full set of assumptions and a complete (and correct) proof?

   Answer: [Yes]

Justification: We provide the full proof of Theorem 1 in the Appendix.

Guidelines:

- The answer NA means that the paper does not include theoretical results.
- All the theorems, formulas, and proofs in the paper should be numbered and cross-referenced.
- All assumptions should be clearly stated or referenced in the statement of any theorems.
- The proofs can either appear in the main paper or the supplemental material, but if they appear in the supplemental material, the authors are encouraged to provide a short proof sketch to provide intuition.
- Inversely, any informal proof provided in the core of the paper should be complemented by formal proofs provided in appendix or supplemental material.
- Theorems and Lemmas that the proof relies upon should be properly referenced.

4. **Experimental Result Reproducibility**

   Question: Does the paper fully disclose all the information needed to reproduce the main experimental results of the paper to the extent that it affects the main claims and/or conclusions of the paper (regardless of whether the code and data are provided or not)?

   Answer: [Yes]

   Justification: Yes, the paper includes a detailed description of the experimental setup, methodology, and parameters used, ensuring that the main experimental results can be reproduced. Additionally, we provide comprehensive technical details in the appendix to support reproducibility.

   Guidelines:

   - The answer NA means that the paper does not include experiments.
   - If the paper includes experiments, a No answer to this question will not be perceived well by the reviewers: Making the paper reproducible is important, regardless of whether the code and data are provided or not.
   - If the contribution is a dataset and/or model, the authors should describe the steps taken to make their results reproducible or verifiable.
   - Depending on the contribution, reproducibility can be accomplished in various ways. For example, if the contribution is a novel architecture, describing the architecture fully might suffice, or if the contribution is a specific model and empirical evaluation, it may be necessary to either make it possible for others to replicate the model with the same dataset, or provide access to the model. In general. releasing code and data is often one good way to accomplish this, but reproducibility can also be provided via detailed instructions for how to replicate the results, access to a hosted model (e.g., in the case of a large language model), releasing of a model checkpoint, or other means that are appropriate to the research performed.
   - While NeurIPS does not require releasing code, the conference does require all submissions to provide some reasonable avenue for reproducibility, which may depend on the nature of the contribution. For example
     (a) If the contribution is primarily a new algorithm, the paper should make it clear how to reproduce that algorithm.
     (b) If the contribution is primarily a new model architecture, the paper should describe the architecture clearly and fully.
     (c) If the contribution is a new model (e.g., a large language model), then there should either be a way to access this model for reproducing the results or a way to reproduce the model (e.g., with an open-source dataset or instructions for how to construct the dataset).
     (d) We recognize that reproducibility may be tricky in some cases, in which case authors are welcome to describe the particular way they provide for reproducibility. In the case of closed-source models, it may be that access to the model is limited in some way (e.g., to registered users), but it should be possible for other researchers to have some path to reproducing or verifying the results.

5. **Open access to data and code**

Question: Does the paper provide open access to the data and code, with sufficient instructions to faithfully reproduce the main experimental results, as described in supplemental material?

Answer: [No]

Justification: We will open-source the code in the future.

Guidelines:

- The answer NA means that paper does not include experiments requiring code.
- Please see the NeurIPS code and data submission guidelines (`https://nips.cc/public/guides/CodeSubmissionPolicy`) for more details.
- While we encourage the release of code and data, we understand that this might not be possible, so "No" is an acceptable answer. Papers cannot be rejected simply for not including code, unless this is central to the contribution (e.g., for a new open-source benchmark).
- The instructions should contain the exact command and environment needed to run to reproduce the results. See the NeurIPS code and data submission guidelines (`https://nips.cc/public/guides/CodeSubmissionPolicy`) for more details.
- The authors should provide instructions on data access and preparation, including how to access the raw data, preprocessed data, intermediate data, and generated data, etc.
- The authors should provide scripts to reproduce all experimental results for the new proposed method and baselines. If only a subset of experiments are reproducible, they should state which ones are omitted from the script and why.
- At submission time, to preserve anonymity, the authors should release anonymized versions (if applicable).
- Providing as much information as possible in supplemental material (appended to the paper) is recommended, but including URLs to data and code is permitted.

6. **Experimental Setting/Details**

   Question: Does the paper specify all the training and test details (e.g., data splits, hyperparameters, how they were chosen, type of optimizer, etc.) necessary to understand the results?

   Answer: [Yes]

   Justification: We provide detailed information on the experimental setup in the implementation details section of the paper. See Sec. C in the Appendix.

   Guidelines:

   - The answer NA means that the paper does not include experiments.
   - The experimental setting should be presented in the core of the paper to a level of detail that is necessary to appreciate the results and make sense of them.
   - The full details can be provided either with the code, in appendix, or as supplemental material.

7. **Experiment Statistical Significance**

   Question: Does the paper report error bars suitably and correctly defined or other appropriate information about the statistical significance of the experiments?

   Answer: [Yes]

   Justification: Please see Sec. 5 and Sec. C.

   Guidelines:

   - The answer NA means that the paper does not include experiments.
   - The authors should answer "Yes" if the results are accompanied by error bars, confidence intervals, or statistical significance tests, at least for the experiments that support the main claims of the paper.
   - The factors of variability that the error bars are capturing should be clearly stated (for example, train/test split, initialization, random drawing of some parameter, or overall run with given experimental conditions).

- The method for calculating the error bars should be explained (closed form formula, call to a library function, bootstrap, etc.)
- The assumptions made should be given (e.g., Normally distributed errors).
- It should be clear whether the error bar is the standard deviation or the standard error of the mean.
- It is OK to report 1-sigma error bars, but one should state it. The authors should preferably report a 2-sigma error bar than state that they have a 96% CI, if the hypothesis of Normality of errors is not verified.
- For asymmetric distributions, the authors should be careful not to show in tables or figures symmetric error bars that would yield results that are out of range (e.g. negative error rates).
- If error bars are reported in tables or plots, The authors should explain in the text how they were calculated and reference the corresponding figures or tables in the text.

8. **Experiments Compute Resources**

   Question: For each experiment, does the paper provide sufficient information on the computer resources (type of compute workers, memory, time of execution) needed to reproduce the experiments?

   Answer:[Yes]

   Justification: Please see Sec. C.

   Guidelines:

   - The answer NA means that the paper does not include experiments.
   - The paper should indicate the type of compute workers CPU or GPU, internal cluster, or cloud provider, including relevant memory and storage.
   - The paper should provide the amount of compute required for each of the individual experimental runs as well as estimate the total compute.
   - The paper should disclose whether the full research project required more compute than the experiments reported in the paper (e.g., preliminary or failed experiments that didn't make it into the paper).

9. **Code Of Ethics**

   Question: Does the research conducted in the paper conform, in every respect, with the NeurIPS Code of Ethics `https://neurips.cc/public/EthicsGuidelines`?

   Answer: [Yes]

   Justification: The research conducted in the paper conforms, in every respect, with the NeurIPS Code of Ethics.

   Guidelines:

   - The answer NA means that the authors have not reviewed the NeurIPS Code of Ethics.
   - If the authors answer No, they should explain the special circumstances that require a deviation from the Code of Ethics.
   - The authors should make sure to preserve anonymity (e.g., if there is a special consideration due to laws or regulations in their jurisdiction).

10. **Broader Impacts**

    Question: Does the paper discuss both potential positive societal impacts and negative societal impacts of the work performed?

    Answer: [Yes]

    Justification: Please see Sec.F.

    Guidelines:

    - The answer NA means that there is no societal impact of the work performed.
    - If the authors answer NA or No, they should explain why their work has no societal impact or why the paper does not address societal impact.

- Examples of negative societal impacts include potential malicious or unintended uses (e.g., disinformation, generating fake profiles, surveillance), fairness considerations (e.g., deployment of technologies that could make decisions that unfairly impact specific groups), privacy considerations, and security considerations.
- The conference expects that many papers will be foundational research and not tied to particular applications, let alone deployments. However, if there is a direct path to any negative applications, the authors should point it out. For example, it is legitimate to point out that an improvement in the quality of generative models could be used to generate deepfakes for disinformation. On the other hand, it is not needed to point out that a generic algorithm for optimizing neural networks could enable people to train models that generate Deepfakes faster.
- The authors should consider possible harms that could arise when the technology is being used as intended and functioning correctly, harms that could arise when the technology is being used as intended but gives incorrect results, and harms following from (intentional or unintentional) misuse of the technology.
- If there are negative societal impacts, the authors could also discuss possible mitigation strategies (e.g., gated release of models, providing defenses in addition to attacks, mechanisms for monitoring misuse, mechanisms to monitor how a system learns from feedback over time, improving the efficiency and accessibility of ML).

11. **Safeguards**

    Question: Does the paper describe safeguards that have been put in place for responsible release of data or models that have a high risk for misuse (e.g., pretrained language models, image generators, or scraped datasets)?

    Answer: [NA]

    Justification: The paper poses no such risks.

    Guidelines:

    - The answer NA means that the paper poses no such risks.
    - Released models that have a high risk for misuse or dual-use should be released with necessary safeguards to allow for controlled use of the model, for example by requiring that users adhere to usage guidelines or restrictions to access the model or implementing safety filters.
    - Datasets that have been scraped from the Internet could pose safety risks. The authors should describe how they avoided releasing unsafe images.
    - We recognize that providing effective safeguards is challenging, and many papers do not require this, but we encourage authors to take this into account and make a best faith effort.

12. **Licenses for existing assets**

    Question: Are the creators or original owners of assets (e.g., code, data, models), used in the paper, properly credited and are the license and terms of use explicitly mentioned and properly respected?

    Answer: [No]

    Justification: The used datasets are publicly available, and widely used in existing VVD methods. Thus, we do not mention the license of the dataset.

    Guidelines:

    - The answer NA means that the paper does not use existing assets.
    - The authors should cite the original paper that produced the code package or dataset.
    - The authors should state which version of the asset is used and, if possible, include a URL.
    - The name of the license (e.g., CC-BY 4.0) should be included for each asset.
    - For scraped data from a particular source (e.g., website), the copyright and terms of service of that source should be provided.

- If assets are released, the license, copyright information, and terms of use in the package should be provided. For popular datasets, `paperswithcode.com/datasets` has curated licenses for some datasets. Their licensing guide can help determine the license of a dataset.
- For existing datasets that are re-packaged, both the original license and the license of the derived asset (if it has changed) should be provided.
- If this information is not available online, the authors are encouraged to reach out to the asset's creators.

13. **New Assets**

    Question: Are new assets introduced in the paper well documented and is the documentation provided alongside the assets?

    Answer: [NA]

    Justification: We will open source the code after the paper is accepted.

    Guidelines:

    - The answer NA means that the paper does not release new assets.
    - Researchers should communicate the details of the dataset/code/model as part of their submissions via structured templates. This includes details about training, license, limitations, etc.
    - The paper should discuss whether and how consent was obtained from people whose asset is used.
    - At submission time, remember to anonymize your assets (if applicable). You can either create an anonymized URL or include an anonymized zip file.

14. **Crowdsourcing and Research with Human Subjects**

    Question: For crowdsourcing experiments and research with human subjects, does the paper include the full text of instructions given to participants and screenshots, if applicable, as well as details about compensation (if any)?

    Answer: [No]

    Justification: The datasets used in this paper, XD-Violence and UCF-Crime, are publicly available and widely used in research. These datasets were collected by their original creators and made accessible for research purposes.

    Guidelines:

    - The answer NA means that the paper does not involve crowdsourcing nor research with human subjects.
    - Including this information in the supplemental material is fine, but if the main contribution of the paper involves human subjects, then as much detail as possible should be included in the main paper.
    - According to the NeurIPS Code of Ethics, workers involved in data collection, curation, or other labor should be paid at least the minimum wage in the country of the data collector.

15. **Institutional Review Board (IRB) Approvals or Equivalent for Research with Human Subjects**

    Question: Does the paper describe potential risks incurred by study participants, whether such risks were disclosed to the subjects, and whether Institutional Review Board (IRB) approvals (or an equivalent approval/review based on the requirements of your country or institution) were obtained?

    Answer: [No]

    Justification: Since we are using datasets that are already publicly available and have been extensively used in previous research, and given that the content does not involve sensitive personal information, this study did not undergo an independent IRB review.

    Guidelines:

    - The answer NA means that the paper does not involve crowdsourcing nor research with human subjects.

- Depending on the country in which research is conducted, IRB approval (or equivalent) may be required for any human subjects research. If you obtained IRB approval, you should clearly state this in the paper.
- We recognize that the procedures for this may vary significantly between institutions and locations, and we expect authors to adhere to the NeurIPS Code of Ethics and the guidelines for their institution.
- For initial submissions, do not include any information that would break anonymity (if applicable), such as the institution conducting the review.